



Experimental investigation on structural evolution of granite at high temperature induced by microwave irradiation

Junsen Zeng^{1,2} · Qijun Hu¹ · Yuan Chen^{1,2} · Xiaoyan Shu^{2,3} · Shunzhang Chen³ · Leping He^{1,4} · Hexi Tang³ · Xirui Lu^{2,3}

Received: 22 June 2018 / Accepted: 6 August 2019 / Published online: 28 August 2019
© Springer-Verlag GmbH Austria, part of Springer Nature 2019

Abstract

The microwave high-temperature irradiation was introduced to deal with the low efficiency of traditional microwave treatments for breaking granite. Structural evolution of granite between 300 °C and 800 °C was assessed through the morphology, mineral characteristics and mechanical performance. A spherical melt cavity with radial cracks formed near the biotite-rich area at 600 °C and the rock completely disintegrated at 800 °C. Intergranular crack was the main mode of micro-cracks. Besides, the micro crack propagation at 600 °C was affected by the distribution and shapes of mineral grains and original cracks. Furthermore, the intergranular crack in the biotite grain boundary induced many secondary smaller cracks. Feldspar and biotite melted at 800 °C. Thus, the melt probably initiated from the cracked-intensive feldspar near biotite-rich area. The uniaxial compressive strength of granite decreased from 88.17 MPa at 25 °C to 18.61 MPa at 800 °C. Between 300 and 600 °C, the decrease in the uniaxial compressive strength was associated with moisture releasing, quartz transition and thermal induced cracks, and 600–800 °C, the decrease was mainly contributed by the partial melt of rock, and magma intruding and solidifying.

Keywords Rock breakage · Granite · Microwave irradiation · High-temperature

Introduction

Rock breakage becomes a significant consideration in underground excavations such as tunneling, mining and deep geological disposal of nuclear waste (Zheng et al. 2017; Hu et al. 2018). Historically, blasting and mechanical methods are the most commonly used techniques in rock breakage (Saiang and Nordlund 2009; Hassani et al. 2016). However, industries

seek new rock breaking techniques to increase excavation progress and reduce energy consumption and cost. Microwave pretreatment to assist conventional mechanical techniques is a promising technique to deal with rock breakage (Hartlieb et al. 2012; Toifl et al. 2016; Lu et al. 2017).

Microwave irradiation of rock is driven by converting the electromagnetic energy into heat (Toifl et al. 2016, 2017; Hartlieb et al. 2017). The amount of heat generated by microwave is associated with power level, exposure time and mineral characteristic (Tang et al. 2016; Hassani et al. 2016; Lu et al. 2017; Zheng et al. 2017). Either a high microwave power level or long exposure time generates more heat. The dielectric properties of rock-forming minerals determine the microwave susceptibility of rock (Nelson et al. 1989; Ulaby et al. 1990). Biotite easily absorbs microwave while most other rock-forming minerals such as quartz and feldspar are weak microwave absorbers (Lu et al. 2017). For a given rock type, the difference in absorbing and converting capacities of minerals induces a non-uniform heating of rock exposed to microwave irradiation. Thermal gradients introduced into the rock generate thermal stress among different minerals (Toifl et al. 2016; Hartlieb et al. 2017). Therefore, two micro-cracking modes, intergranular and transgranular crack, are

Editorial handling: D. Paktunc

✉ Xirui Lu
luxiruimvp116@163.com

¹ School of Civil Engineering and Architecture, Southwest Petroleum University, Chengdu 610500, People's Republic of China

² State Key Laboratory of Environment-friendly Energy Materials, Southwest University of Science and Technology, Mianyang 621010, People's Republic of China

³ Fundamental Science on Nuclear Wastes and Environmental Safety Laboratory, Southwest University of Science and Technology, Mianyang 621010, People's Republic of China

⁴ State Key Laboratory of Oil and Gas Geology and Exploitation, Chengdu 610500, People's Republic of China

induced when the stress exceeded fracture strength (Wanne and Young 2008; Wang et al. 2008; Meisels et al. 2015; Zheng et al. 2017). Furthermore, anisotropic mineral expansion and quartz α - β transition also promote crack extension (Vázquez et al. 2015; Shcherbakov et al. 2015; Sun et al. 2017; Becattini et al. 2017; Toifl et al. 2017). Moreover, numerous microcracks will develop into a large crack network and significantly weaken the rock strength.

Granite, a weak microwave absorber, is a common rock type in underground excavation. High temperatures (over 800 °C) can stimulate the granite to crack by conventional heating methods (Wang et al. 2013; Guo et al. 2017; Chen et al. 2017). However, the maximum temperatures of granite irradiated by microwave were generally below 400 °C and exhibited a low degree of damage (Hassani et al. 2016; Lu et al. 2017). One of the factors is the weak microwave susceptibility of granite. Furthermore, these works were lack of thermal preservation that induced high heat loss. Considering the closed operating environment of tunnel boring machine, solution to the low degree of damage of granite irradiated by microwave may be inspired from our previous study about the microwave high-temperature sintering treatment for disposing radioactive soil (Zhang et al. 2017). Although some researchers declared that the microwave-irradiated rock breakage relied on the thermal mismatch to induce cracks instead of overall heating, the irradiated rock areas with different temperatures indeed presented variety degrees of crack or melt (Hassani et al. 2016; Zheng et al. 2017). To the best of our knowledge, only a few studies investigated the relationship between damage and temperature of granite irradiated by microwave.

Main purpose of our study is to qualitatively investigate the structural evolution of microwave-irradiated granite with increased temperatures based on changes in morphology, mineral characteristics and mechanical performance.

Materials and methods

Sample properties

A white-black granite was sampled from the Nyainqentanglha mountain in Tibet, China. According to Liu et al. (2005), the granite with the SHRIMP U-Pb age of 11.1 Ma was the product of post-collision tectonic-magmatic activity in Miocene epoch.

Petrographic assessment of a polished block 48 × 28 × 6 mm using a Leitz Laborlux 12 pol optical polarizing microscope, as shown in Fig. 1. Digital images were analyzed with Wisisoft Co and the abbreviation for name of rock-forming minerals were according to Whitney and Evans (2010). The rock consists of 56 vol% alkali-feldspar (partially sericitized), 12 vol% plagioclase (partially saussuritized), 25 vol% quartz,

5 vol% biotite (partially altered to chlorite) and 1 vol% amphibole. Trace minerals 1 vol% include titanite, tourmaline, apatite and zircon.

A PANalytical Axios wavelength-dispersive X-ray fluorescence spectrometer (XRF) instrument was used to determine the chemical composition of granite, as listed in Table 1. For XRF analysis, granite sample powders were pressed into tablets. The declared detection of limit was 0.01 wt% for main elements.

Experimental design and specimen preparation

Considering the dimension of microwave cavity, granite samples were cut as a cube of 20 mm on edge using a circular diamond blade. Each specimen consisted of three individual cubes to enhance mineralogical representativity as largely determined by grain size. Only cubes without any visible cracks were used in the irradiation experiments, to minimize influence of initial crack present. All specimens were dried at 110 °C for 12 h in a conventional oven to eliminate the influence of moisture.

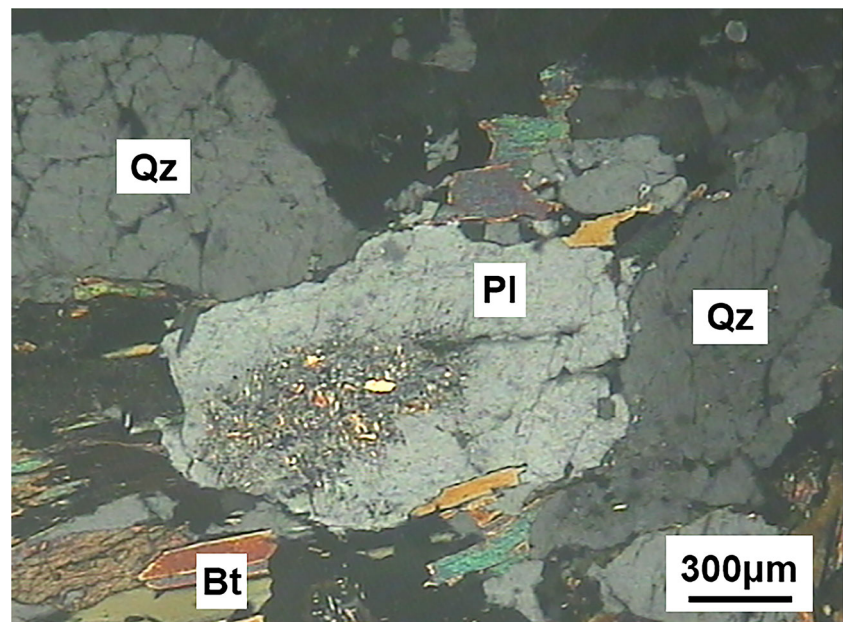
According to the microwave propagation pattern within the sample inside the closed cavity (Hassani et al. 2016), both microwave intensity and resultant temperature decay with increasing distance from the antenna mound. Samples were placed individually in a cavity within refractory alumina (Al₂O₃) brick to ensure uniform exposed of all cubes to the microwave radiation, as well as to protect the equipment from contact with molten material. Final surface temperatures of the irradiated rock sample were preset to cover the interval 300–800 °C at 100 °C increments, as previously described in the experiments by Zheng et al. (2017; see Fig. 2). It is quite possible that the interior temperature within the cubes is higher, as seems to be implied by the extrusion of molten material at the highest temperature settings.

Specimens were heated to preset temperatures with the same heating rate of 7 °C/min and then kept for 15 min. This condition was determined by a large number of previous experiments to keep the temperature stably rising and to avoid the melting of large area due to internal heat accumulation at high temperatures, respectively. After 15 min at the preset temperature, the power supply was switched off, and specimens were allowed to cool to room temperature in the furnace at a rate of 3 °C/min.

Scanning electronic microscopy (SEM)

In-situ observation of sample material morphology before and after microwave exposure was assessed in a Hitachi TM4000 scanning electron microscope (SEM). Sample material was mounted on an aluminum stub with electrically conductive carbon tape, and sputtered with 10 nm metallic gold using Cressington 208HR equipment. The instrument was operated

Fig. 1 Petrographic microscopy images obtained from Nyainqentanglha granite (Qz-quartz; Pl-plagioclase; Bt-biotite)



in high vacuum mode ($<10^{-6}$ Torr) at 15 kV, with a beam current between 6.6–6.9 nA (on Faraday cup) and working distance of 5.8–6.7 mm. Some of the samples were studied in a KYKY EM8000F Schottky FE-SEM instrument, operated in high vacuum at 10 kV and 5 nA, with a working distance of 20 mm.

Thermal analysis

Thermogravimetric analysis (TGA) and differential-scanning calorimetry (DSC) were done in a TA Instruments SDT Q160 simultaneous thermal analyzer. Powdered sample material 8.84 mg was heated at 10 °C/min over a temperature range from 25 to 800 °C in air. Raw data processing and correction were done using TA Q series Advantage Universal Analysis proprietary software.

X-ray powder diffraction (XRPD)

Samples for X-ray powder diffraction analysis (XRPD) were prepared from cube specimens after completed uniaxial compressive-strength testing. Crushed samples were further comminuted and pulverized under acetone in an agate mortar and pestle. Powders were front-loaded in a 25 mm diameter dimpled glass specimen holder.

Diffractograms were recorded in PANalytical X'Pert PRO X-ray diffractometer instrument using bulk, non-filtered, non-monochromated $\text{CuK}\alpha$ radiation of $\lambda = 1.54184$ Å. The XRD pattern was recorded from 3 to 80 °2 θ at a scanning rate of 5 °2 θ /min, total scan duration 15m36s. Diffractograms were evaluated using JADE software, to determine mineral modal contents in wt% of the granite sample material.

Uniaxial compressive-strength testing

Uniaxial compressive strength was used to evaluate the mechanical performance of cubic specimens after microwave treatment. The uniaxial compressive testing for 21 cube specimens was carried out at a constant loading rate of 0.3 kN/s through a Wuxi Jianyi Instrument & Machinery Co. Ltd. TYE-300 uniaxial compressive machine with a V2.0 data recorder. The sample platen was cleaned before each test; post-testing sample remains were collected for analysis by XRPD (see above).

Microwave high-temperature irradiation

The SYNOTHERM HAMiLab-M1500 microwave high-temperature heating furnace (2.45 GHz) consists of a control system, single magnetron, metal-clad interior

Table 1 Results of XRF analysis of Nyainqentanglha granite sample

Constituent	SiO ₂	K ₂ O	Al ₂ O ₃	Fe ₂ O ₃	CaO	TiO ₂	Na ₂ O	P ₂ O ₅	MgO	BaO
Content (wt%)	65.65	11.20	10.93	4.97	4.11	1.00	0.62	0.36	0.34	0.27
Constituent	SrO	MnO	ZrO ₂	Cl	SO ₃	Rb ₂ O	ZnO	ThO ₂	Y ₂ O ₃	Total
Content (wt%)	0.14	0.10	0.08	0.07	0.07	0.06	0.02	0.02	0.01	100.02

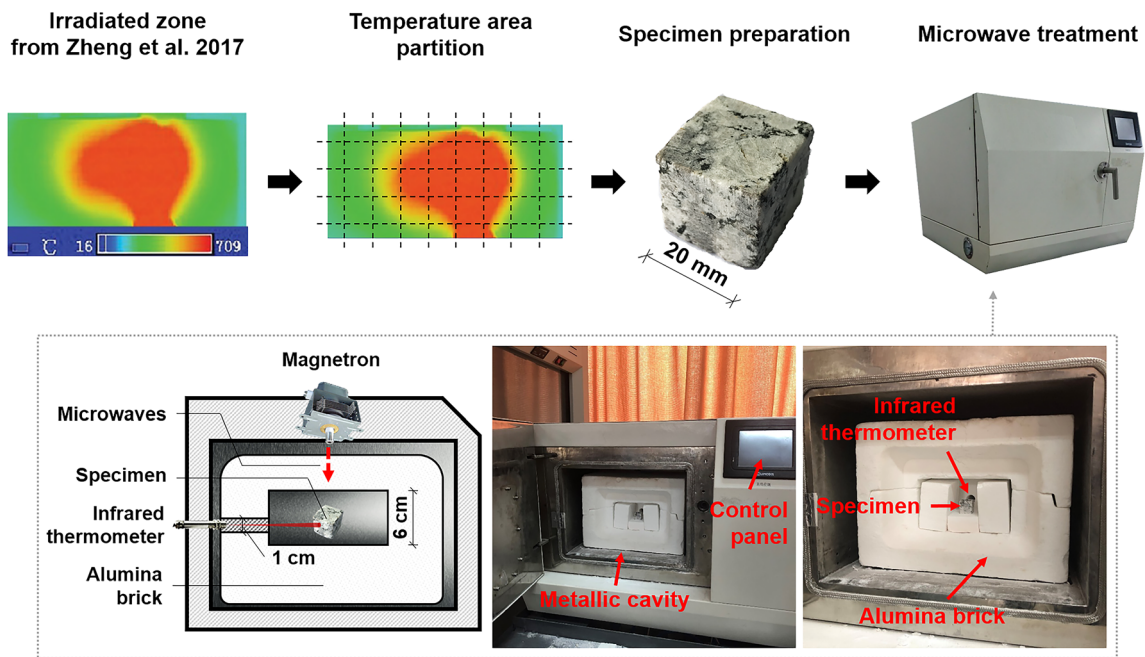


Fig. 2 Schematic of the experimental design and microwave instrument

cavity, and an alumina refractory brick filling most of the cavity to position samples at uniform distance from the microwave antenna mound, also holding an infrared thermometer in a special recess close to the sample.

Microwave radiation was generated from the magnetron source mounted above the cavity. Output power is adjustable from 1.4 kW (=nominal output power of the magnetron tube) downward by operating the tube intermittently at longer or shorter intervals so that output power is reduced when integrated over time.

Alumina is refractory and transparent to microwave radiation, and was selected for thermal insulation during microwave function, as well as to protect the oven interior from potentially hot lava splatter if sample cubes should melt or disintegrate. Specimen cubes were positioned in the cavity in the alumina brick with one face towards the infrared thermometer to ensure correct instrument reading. The range of infrared thermometer was 250–1650 °C with an accuracy of ± 0.1 °C.

Results

Cube appearance and morphology

Figures 3 and 4 show the cube specimens at different temperatures. With increasing temperature, color of the specimen changed, especially biotite changed from black to brown

(see in Fig. 4c). Visible cracks appeared in the cube edges at 500 °C. Subsequently, the minerals near the biotite-rich area melted and formed a spherical cavity at 600 °C (Fig. 4a). In addition, radially oriented cracks originating from the boundary of cavity and volume expansion were also observed at 600 °C. Between 600 and 800 °C, besides the increase of cracking density, the melt cavity also enlarged and melted minerals formed black glass which contained bubbles and small particles.

Micromorphology by SEM

Figure 5 reveals the micromorphology of the specimen surface after microwave exposure to 600 °C, and melted minerals at 800 °C. After microwave exposure, intergranular cracking was observed to occur along the grain boundary of biotite, with subordinate transgranular cracking. Cracking appears to further extend the pre-existing cracks. Furthermore, a number of smaller secondary cracks formed in the surrounding minerals due to intergranular crack forming (Fig. 5d and f). Intergranular cracks occur mainly in fine-grained parts of the rock, whereas transgranular cracks are only observed in coarse mineral grains. Cracks in biotite do follow the main cleavage direction, but may have existed prior to microwave exposure, which we were unable to confirm. Figure 5g and h reveal the presence of glass blebs deposited on the sample surface as well as melt pits after exposure to 800 °C.

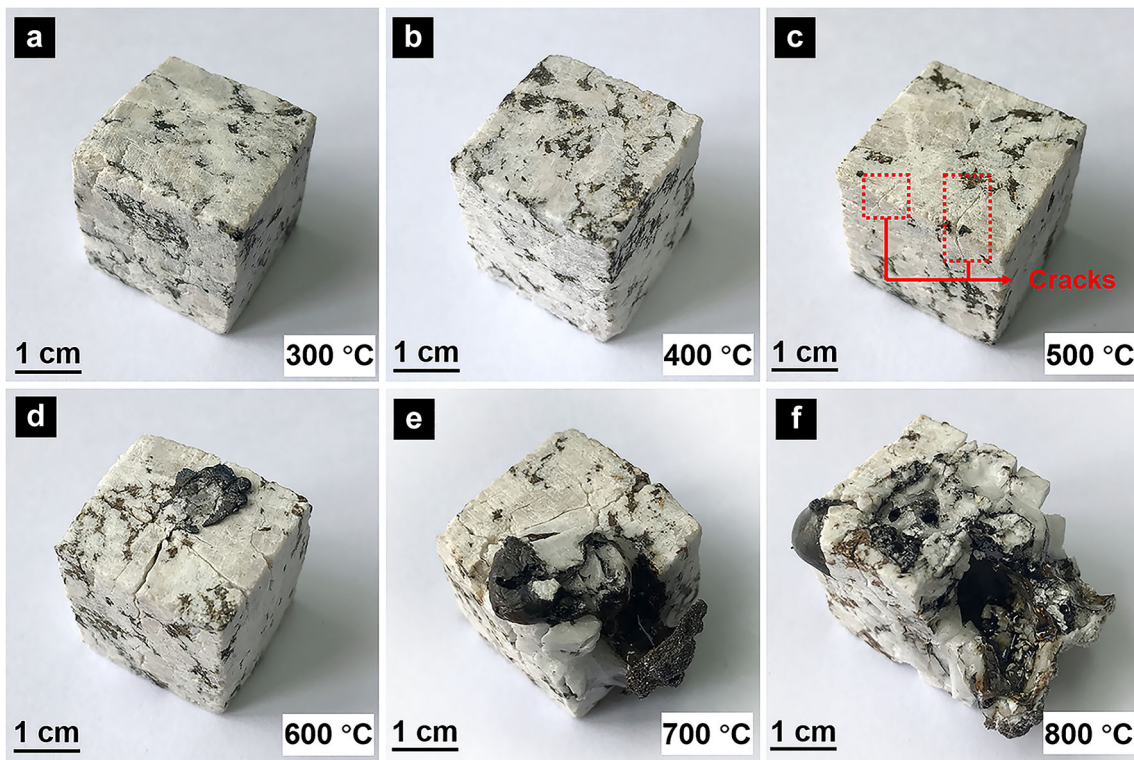


Fig. 3 Morphologies of irradiated specimen at different temperatures

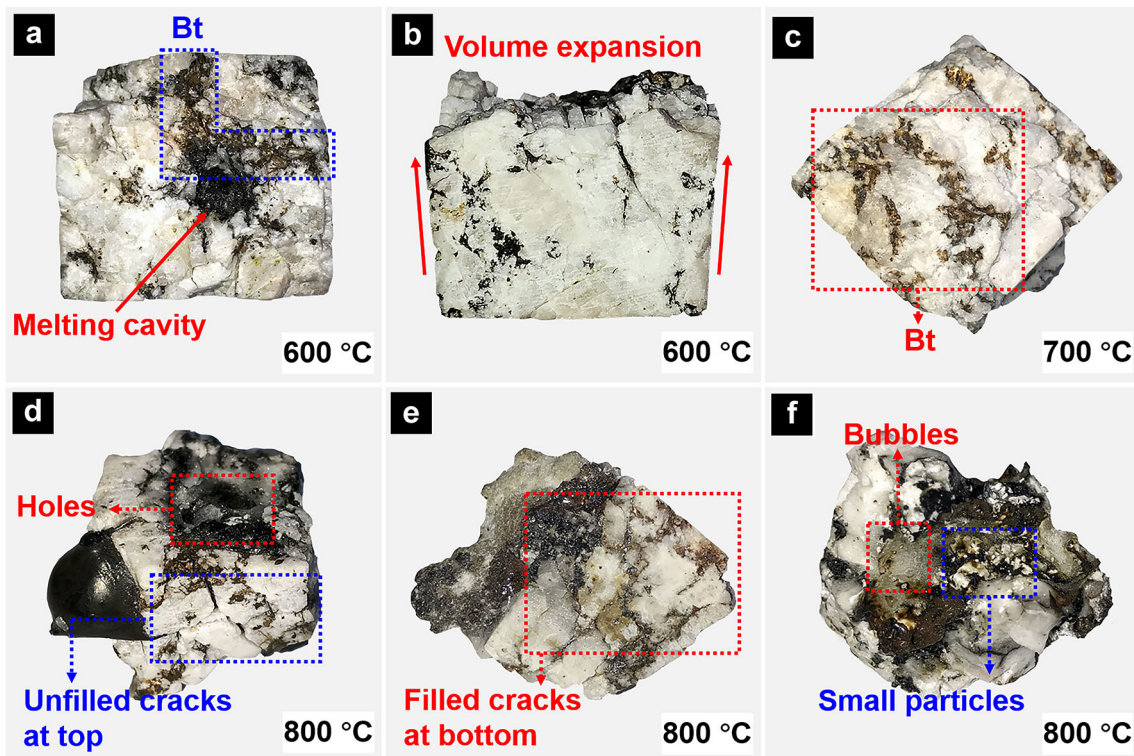
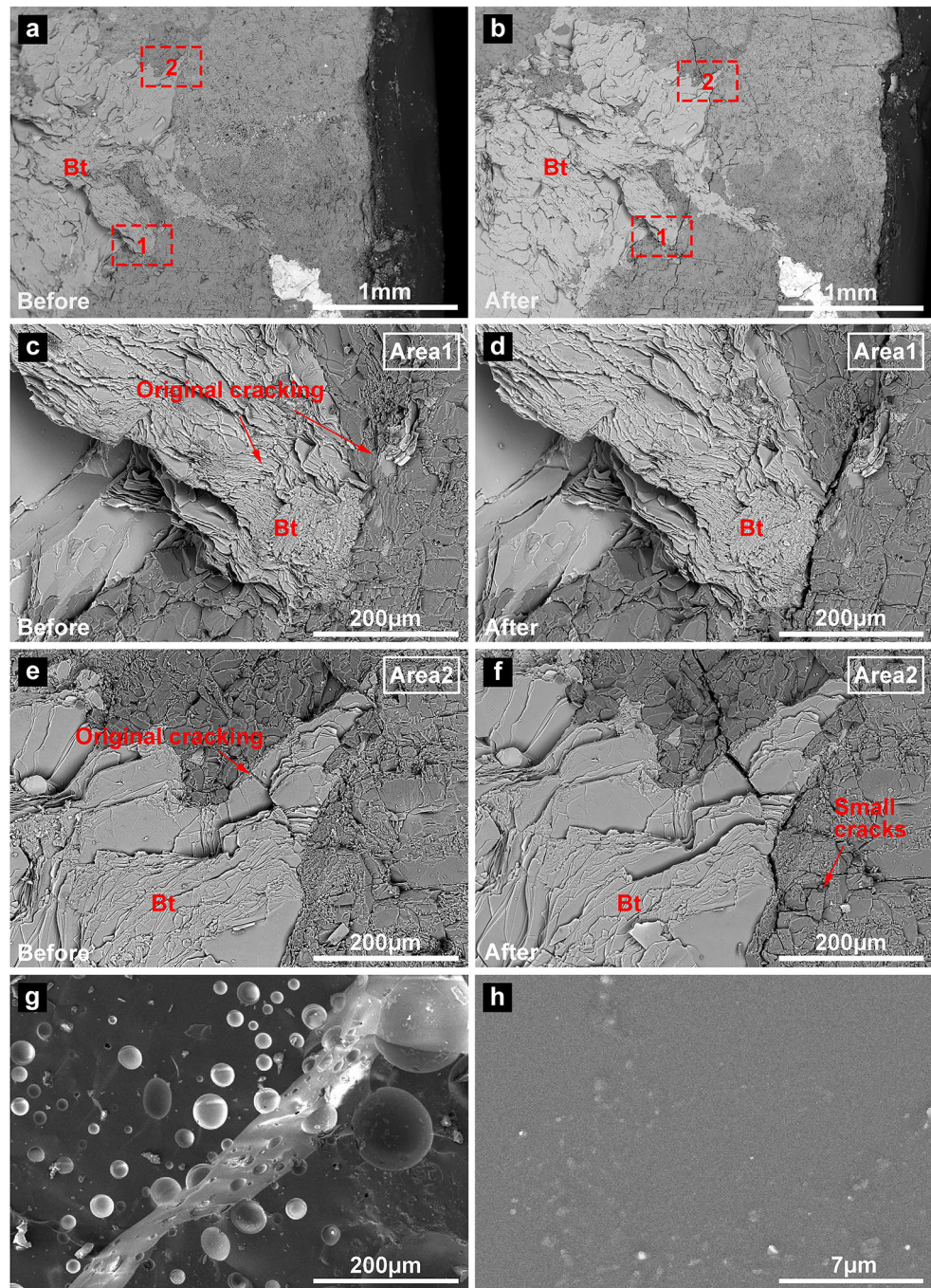


Fig. 4 Details of specimens after irradiation at different temperatures

Fig. 5 SEM pictures of: **a–f** the in-situ observation of specimen surface before and after microwave irradiation with a maximum temperature of 600 °C; **g** and **h** the surface of melted minerals at 800 °C



Uniaxial compressive-strength testing

Figure 6 presents the variation in uniaxial strength in MPa of cubic specimens before and after microwave irradiation. We employed cubic polynomial to fit the curve whose coefficient of determination of 0.90241. Compressive strength significantly decreased from 88.17 MPa at 25 °C to 18.61 MPa at 800 °C. For temperature below 600 °C, compressive strength decreased almost linearly, whereas between 600 and 800 °C it slowed down. Besides, the variability in

results was large but declined gradually as temperature increased.

Thermal analysis by TGA-DSC

Figure 7 shows the TG-DSC curves of untreated granite. The maximum mass loss of granite sample is approximately 0.6 wt% at 700 °C. Between 700 °C and 800 °C, the mass no longer varied. Besides, the small endothermic peak about 570 °C at the heat flow curve was the α - β quartz transition at 573 °C (Plevova et al. 2016).

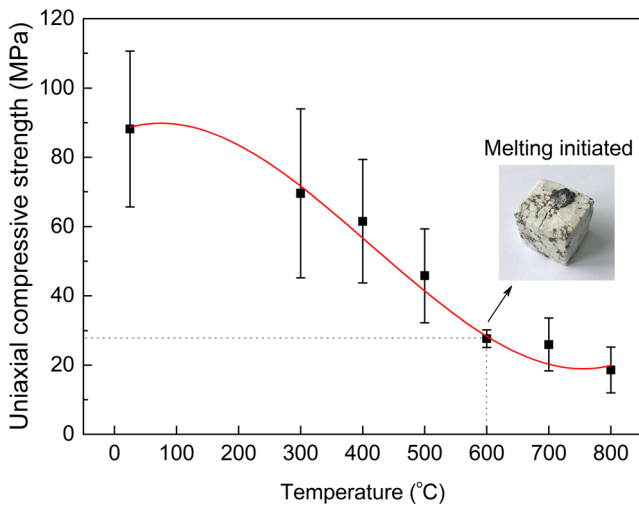


Fig. 6 Uniaxial compressive strength of granite specimen before and after microwave treatment

X-ray powder diffraction (XRPD)

Figure 8 presents the diffractograms of powdered rock samples before and after microwave irradiation at different surface temperatures. The mineral composition was unchanged while some crystal mineral phases varied as temperature increased. The intensity of quartz diffraction peaks almost maintained before and after microwave irradiation. The intensity of biotite diffraction peak at $8.8^\circ 2\theta$ increased between 25 and 600 °C and decreased over 600 °C with the peak synchronously shifting to the large angle. At 800 °C, both biotite and feldspar diffraction peaks almost vanished.

Discussion

Propagation of crack and melt

Temperature below 500 °C hardly generated visible damage in granite. Visible cracks appeared in the cube edge at 500 °C

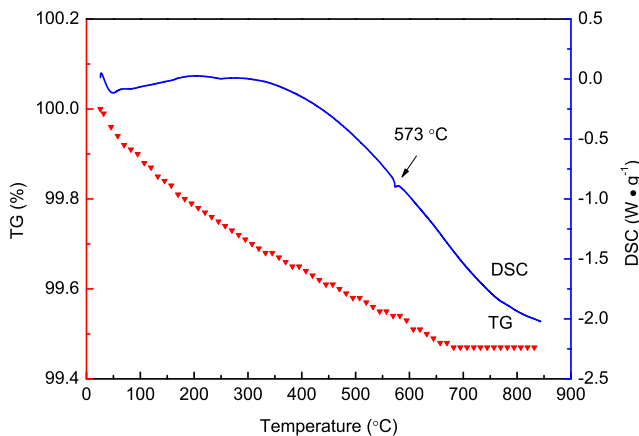


Fig. 7 TG-DSC curves of Nyainqentanglha granite

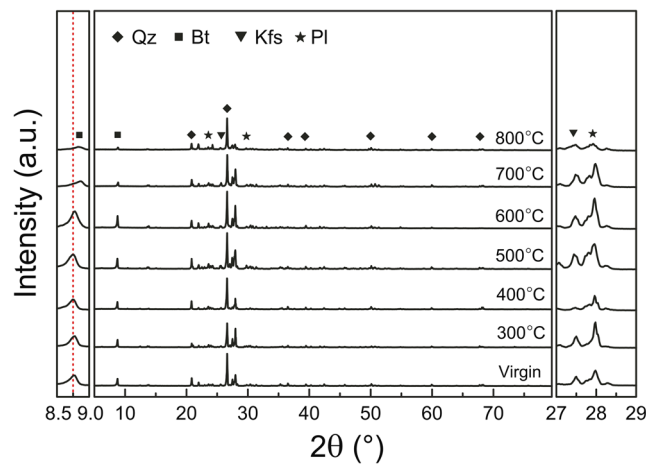


Fig. 8 Powder XRD patterns obtained from specimens before and after microwave irradiation

because the thermal stress easily concentrated at the corner of particle (Zhu et al. 2017). This can also explicate the micro crack propagation at 600 °C. Although the initial direction of main crack was difficult to identify, the crack propagation could be summarized. Since microwave susceptibility of biotite was higher than most of other mineral components in granite, thermal stress easily concentrated at grain boundaries between biotite and surrounding minerals, so that the main crack was close to biotite. Besides, position and direction of original cracks also affected the pattern of main crack. Secondary cracks in the mineral near biotite probably lead to the further damage in granite at high temperatures. Intergranular crack destroyed the original stable state of minerals near the biotite. Besides, the heterogeneous volume expansion between the biotite and surrounding minerals may also induce the radial fracture. These secondary cracks split the surrounding minerals into pieces and possibly caused these small particles easier to melt with temperature increasing. Therefore, the spherical melt cavity probably originated from the crack-intensive minerals (quartz or feldspar) near biotite-rich area. Subsequently, radial micro-cracks formed affected by thermal stress concentration (Zuo et al. 2017) and gradually developed into the macro-cracks in Fig. 4a. Eventually, continuous microwave irradiation offered the required energy for the enlargement of melt cavity and crack network, accelerating the disintegration of specimen above 600 °C.

Evolution of mineral characteristics

The process of crack to partial melt occurred between 500 and 600 °C (surface) according to macro damage, while the internal temperature was unable to measure. Thus, we considered to use TG-DSC and XRPD to assess the internal temperature as well as evolution of mineral characteristics. Due to the chemical inertness of granite, the mass loss could be associated with the liberating of pore water and water-bearing mineral

(Zhang et al. 2016; Chen et al. 2017). Further mass decline over 650 °C possibly was associated with the dehydroxylation of biotite (Labus 2017). Since only quartz existed distinctly in the melted minerals at 800 °C, the internal maximum temperature was probably between 1400 and 1750 °C, which was the melt point of feldspar and quartz respectively (Jiang et al. 2015). For biotite, the increase of diffraction peak intensity between 400 and 600 °C revealed that the crystal was transformed into a more stable structure (Chen et al. 2017). The displacement of biotite diffraction peak over 600 °C indicated the unit cell shrinking which may induce the transgranular cracking in biotite. As the dehydroxylation finished over 700 °C, biotite melted and was further converted to glass. For feldspar, the distinct decrease of diffraction peaks intensities at 800 °C also revealed the partial melt. Moreover, the water content increasing due to the plagioclase partially altered to sericite, may also stimulate the plagioclase to disintegrate. Therefore, the molten minerals mainly consist of feldspar and biotite.

Reduction of mechanical performance

Combined with results, the decrease between 300 and 600 °C was affected by moisture releasing, quartz transition and thermal induced crack. Particularly, between 400 and 600 °C, crack gradually became the main factor in granite damaging. To date, the mechanical performances of rock was most influenced by quartz (Tiskatine et al. 2016; Chen et al. 2017). The quartz transformed from trigonal α -phase to hexagonal β -phase at 573 °C accompanying by a significant change trended towards higher symmetry and volume (Vázquez et al. 2015). Since the temperature exceeded the threshold, a number of micro-cracks occurred. Besides, the quartz transition was reversible in cooling stage, which presumably led

cracks to further extend (Chao et al. 2017; Sun et al. 2017). For temperature ranging from 600 to 700 °C, the downtrend slowing was probably because some cracks were filled with magma, which slightly increased the structural integrity in the cooling stage. However, the downtrend seemed to be overwhelming due to the vast melt cavity and crack network at 800 °C. The variability of uniaxial compressive strength was primarily due to the non-uniform heating contributed by the change of mineralogical representability as largely determined by grain size.

Failure mechanism at high temperatures

Figure 9 further illustrates the failure mechanism of granite at high temperatures irradiated by microwaves. Melt pockets firstly occurred at the corner of particles and then formed a film which wrapped up the particle isolated by cracks (Jin et al. 1994; Zhu et al. 2011). Although the internal temperature was difficult to identify, the melt cavity was considered to be originated from the crack-intensive feldspar near the biotite-rich area according to SEM and XRPD results. Over 600 °C, the melt and crack extending further accelerated the structural disintegration. On one hand, scorching steam gushed upward to soften and melt the top minerals. Once the holes formed, the steam escaped and the top softened minerals would collapse toward the center so that induced the top cracks significantly to broaden. On the other hand, the magma flowed into the bottom cracks and filled which up. With the magma continuously intruding into crack-intensive area, the magma conduit formed and the small particles were carried by magma. Therefore, the combined effect, which was partial melt of granite, and magma intruding and solidifying, took the main parts for damaging the granite structure above 600 °C.

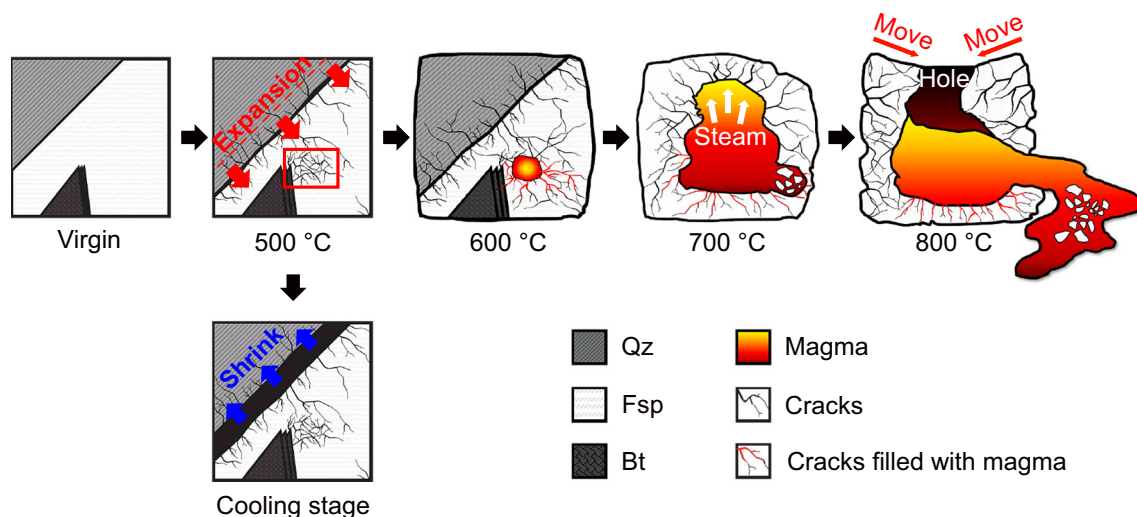


Fig. 9 Schematic diagram of failure mechanism on granite irradiated by microwave

Conclusions

The feasibility of microwave high-temperature heating on granite were studied. Furthermore, the structural evolution of microwave-irradiated granite in 300–800 °C was investigated based on changes of morphology, mineral characteristics and mechanical performance. In this study, some basic conclusions can be drawn as follows:

- (1) A spherical melt cavity with distinct radial cracks formed near the biotite-rich area at 600 °C and the rock completely disintegrated at 800 °C.
- (2) SEM observed both transgranular and intergranular cracking modes, but the latter one dominated. Besides, the micro crack propagation at 600 °C was affected by the distribution and shapes of mineral grains and original cracks. Furthermore, the intergranular crack in the biotite grain boundary induced many secondary smaller cracks which split the mineral near biotite into pieces.
- (3) TG-DSC detected the moisture releasing and α - β quartz transition. XRPD results revealed feldspar and biotite melted at 800 °C. Combined with SEM and XRPD results, the melt cavity probably originated from the crack-intensive feldspar near biotite-rich area.
- (4) The uniaxial compressive strength of granite declined from 88.17 MPa at 25 °C to 18.61 MPa at 800 °C. Between 300 and 600 °C, the decrease was associated with moisture releasing, quartz transition, and thermal induced cracks; and 600–800 °C, it was mainly contributed by the partial melt, flow and solidification of minerals.

Acknowledgements This research was supported by the National Natural Science Foundation of China (51574201, 21677118), the Doctor Research Foundation of Southwest University of Science and Technology (18zx7141). The authors would like to express sincere gratitude to Lanjie Hou of Key Laboratory of Solid Waste Treatment and Resource Recycle Ministry of Education for the help in rock mineralogical analysis.

References

- Becattini V, Motmans T, Zappone A, Madonna C, Haselbacher A, Steinfeld A (2017) Experimental investigation of the thermal and mechanical stability of rocks for high-temperature thermal-energy storage. *Appl Energy* 203:373–389
- Chao L, Sun Q, Zhang W, Geng J, Qi Y, Lu L (2017) The effect of high temperature on tensile strength of sandstone. *Appl Therm Eng* 111: 573–579
- Chen YL, Wang SR, Ni J, Azzam R, Fernández-Steese TM (2017) An experimental study of the mechanical properties of granite after high temperature exposure based on mineral characteristics. *Eng Geol* 220:234–242
- Guo H, Guo W, Zhai Y, Su Y (2017) Experimental and modeling investigation on the dynamic response of granite after high-temperature treatment under different pressures. *Constr Build Mater* 155:427–440
- Hartlieb P, Leindl M, Kuchar F, Antretter T, Moser P (2012) Damage of basalt induced by microwave irradiation. *Miner Eng* 31(3):82–89
- Hartlieb P, Grafe B, Shepel T, Malovyk A (2017) Experimental study on artificially induced crack patterns and their consequences on mechanical excavation processes. *Int J Rock Mech Min Sci* 100:160–169
- Hassani F, Nekoovaght PM, Gharib N (2016) The influence of microwave irradiation on rocks for microwave-assisted underground excavation. *J Rock Mech Geotech Eng* 8(1):1–15
- Hu Q, Zeng J, Wang L, Shu X, Shao D, Zhang H, Lu X (2018) Helium ion irradiation effects on neodymium and cerium co-doped $Gd_2Zr_2O_7$ pyrochlore ceramic. *J Rare Earths* 36:398–403
- Jiang H, Lee CTA, Morgan JK, Rose CH (2015) Geochemistry and thermodynamics of an earthquake: a case study of pseudotachylites within mylonitic granitoid. *Earth Planet Sci Lett* 430:235–248
- Jin ZM, Green HW, Zhou Y (1994) Melt topology in partially molten mantle peridotite during ductile, deformation. *Nature* 372(6502): 164–167
- Liu Q, Wu Z, Ye P, Hu D, Jiang W, Ke D, Zhang H (2005) Isotopic dating of the Nyainqentanglha granite and its significance. *Acta Geol* 79(3):331–337 [In Chinese]
- Lu GM, Li YH, Hassani F, Zhang X (2017) The influence of microwave irradiation on thermal properties of main rock-forming minerals. *Appl Therm Eng* 112:1523–1532
- Labus M (2017) Thermal methods implementation in analysis of fine-grained rocks containing organic matter. *Journal of Thermal Analysis and Calorimetry* 129 (2):965–973
- Meisels R, Toifl M, Hartlieb P, Kuchar K, Antretter T (2015) Microwave propagation and absorption and its thermo-mechanical consequences in heterogeneous rocks. *Int J Miner Process* 135(3):40–51
- Nelson SO, Lindroth DP, Blake RL (1989) Dielectric properties of selected minerals at 1 to 22 GHz. *Geophysics* 54(10):1344–1349
- Plevova E, Vaculikova L, Kozusnikova A, Ritz M, Martynkova GS (2016) Thermal expansion behaviour of granites. *J Therm Anal Calorim* 123(2):1555–1561
- Saiang D, Nordlund E (2009) Numerical analyses of the influence of blast-induced damaged rock around shallow tunnels in brittle rock. *Rock Mech Rock Eng* 42(3):421–448
- Shcherbakov IP, Kuksenko VS, Chmel' AE (2015) Role of water impurity in impact fracture of quartz in the vicinity of the phase transition at 573°C. *Tech Phys* 60(9):1405–1409
- Sun H, Sun Q, Deng W, Zhang W, Lü C (2017) Temperature effect on microstructure and p-wave propagation in Linyi sandstone. *Appl Therm Eng* 115:913–922
- Tang Y, Xu G, Qu C, Sun L, Duan Y (2016) Damage simulation of a random aggregate model induced by microwave under different discontinuous ratios and exposure times. *Adv Mater Sci Eng* 2016:1–11
- Tiskatine R, Eddemani A, Gourdo L, Abnay B, Ihlal A, Aharoune A, Bouirden L (2016) Experimental evaluation of thermo-mechanical performances of candidate rocks for use in high temperature thermal storage. *Appl Energy* 171:243–255
- Toifl M, Meisels R, Hartlieb P, Kuchar F, Antretter T (2016) 3D numerical study on microwave induced stresses in inhomogeneous hard rocks. *Miner Eng* 90:29–42
- Toifl M, Hartlieb P, Meisels R, Antretter T, Kuchar K (2017) Numerical study of the influence of irradiation parameters on the microwave-induced stresses in granite. *Miner Eng* 103-104:78–92
- Ulaby FT, Sarabandi K, McDonald K, Whitt M, Dobson MC, Sieber AJ (1990) Michigan microwave canopy scattering model. *Int J Remote Sens* 11(7):1223–1253
- Vázquez P, Shushakova V, Gómez-Heras M (2015) Influence of mineralogy on granite decay induced by temperature increase: experimental observations and stress simulation. *Eng Geol* 189:58–67
- Wang G, Radziszewski P, Ouellet J (2008) Particle modeling simulation of thermal effects on ore breakage. *Comput Mater Sci* 43(4):892–901

- Wang XQ, Schubnel A, Fortin J, Guéguen Y, Ge HK (2013) Physical properties and brittle strength of thermally cracked granite under confinement. *J Geophys Res Solid Earth* 118(12):6099–6112
- Wanne TS, Young RP (2008) Bonded-particle modeling of thermally fractured granite. *Int J Rock Mech Min Sci* 45(5):789–799
- Whitney DL, Evans BW (2010) Abbreviations for names of rock-forming minerals. *Am Mineral* 95:185–187
- Zhang W, Sun Q, Hao S, Geng J, Lv C (2016) Experimental study on the variation of physical and mechanical of rock after high temperature treatment. *Appl Therm Eng* 98:1297–1304
- Zhang S, Shu X, Chen S, Yang H, Hou C, Mao X, Chi F, Song M, Lu X (2017) Rapid immobilization of simulated radioactive soil waste by microwave sintering. *J Hazard Mater* 337:20–26
- Zheng YL, Zhang QB, Zhao J (2017) Effect of microwave treatment on thermal and ultrasonic properties of gabbro. *Appl Therm Eng* 127: 359–369
- Zhu W, Gaetani GA, Fusses F, Montési LG, De Carlo CF (2011) Microtomography of partially molten rocks: three-dimensional melt distribution in mantle peridotite. *Science* 332(6025):88–91
- Zhu S, Zhang W, Sun Q, Deng S, Geng J, Li C (2017) Thermally induced variation of primary wave velocity in granite from Yantai: experimental and modeling results. *Int J Therm Sci* 114:320–326
- Zuo JP, Wang JT, Sun YJ, Chen Y, Jiang GH, Li YH (2017) Effects of thermal treatment on fracture characteristics of granite from Beishan, a possible high-level radioactive waste disposal site in China. *Eng Fract Mech* 182:425–437

Publisher's note Springer Nature remains neutral with regard to jurisdictional claims in published maps and institutional affiliations.